



LAWRENCE
LIVERMORE
NATIONAL
LABORATORY

Dead Zones in LX-17 and PBX 9502

P. Clark Souers, Henry G. Andreski, Jan Batteux, Brad Bratton, Chris Cabacungan, Charles F. Cook, III, Sabrina Fletcher, Raul Garza, Denise Grimsley, Jeff Handly, Andy Hernandez, Pat McMaster, John D. Molitoris, Rick Palmer, Jim Prindiville, John Rodriguez, Dan Schneberk, Bradley Wong, Peter Vitello

September 9, 2005

Propellants, Explosives, Pyrotechnics

Disclaimer

This document was prepared as an account of work sponsored by an agency of the United States Government. Neither the United States Government nor the University of California nor any of their employees, makes any warranty, express or implied, or assumes any legal liability or responsibility for the accuracy, completeness, or usefulness of any information, apparatus, product, or process disclosed, or represents that its use would not infringe privately owned rights. Reference herein to any specific commercial product, process, or service by trade name, trademark, manufacturer, or otherwise, does not necessarily constitute or imply its endorsement, recommendation, or favoring by the United States Government or the University of California. The views and opinions of authors expressed herein do not necessarily state or reflect those of the United States Government or the University of California, and shall not be used for advertising or product endorsement purposes.

Dead Zones in LX-17 and PBX 9502

P. Clark Souers*, Henry G. Andreski, Jan Batteux, Brad Bratton, Chris Cabacungan, Charles F. Cook III, Sabrina Fletcher, Raul Garza, Denise Grimsley, Jeff Handly, Andy Hernandez, Pat McMaster, John D. Molitoris, Rick Palmer, Jim Prindiville, John Rodriguez, Dan Schneberk, Bradley Wong, and Peter Vitello

Energetic Materials Center, Lawrence Livermore National Laboratory, Livermore, CA USA 94550

Corresponding author; e-mail: souers1@llnl.gov

Abstract

Pin and X-ray corner-turning data have been taken on ambient LX-17 and PBX 9052, and the results are listed in tables as an aid to future modeling. The results have been modeled at 4 zones/mm with a reactive flow approach that varies the burn rate as a function of pressure. A single rate format is used to simulate failure and detonation in different pressure regimes. A pressure cut-off must also be reached to initiate the burn. Corner-turning and failure are modeled using an intermediate pressure rate region, and detonation occurs at high pressure. The TATB booster is also modeled using reactive flow, and X-ray tomography is used to partition the ram-pressed hemisphere into five different density regions. The model reasonably fits the bare corner-turning experiment but predicts a smaller dead zone with steel confinement, in contradiction with experiment. The same model also calculates the confined and unconfined cylinder detonation velocities and predicts the failure of the unconfined cylinder at 3.75 mm radius. The PBX 9502 shows a smaller dead zone than LX-17. An old experiment that showed a large apparent dead zone in Comp B was repeated with X-ray transmission and no dead zone was seen. This confirms the idea that a variable burn rate is the key to modeling. The model also produces initiation delays, which are shorter than those found in time-to-detonation.

Keywords: dead zone, corner-turning, X-ray, failure, reactive flow

1 Introduction

Abrupt corner-turning of detonation was first studied as the detonation moved from a near-ideal cylinder of small radius suddenly into a cylinder of large radius as seen at the left in Figure 1 [1-3]. Refinements were made to the double-cylinder in order to obtain maximum data from the breakout of the detonation on the edges. Enough delay was seen that dead zones, or regions of no detonation, were postulated. The coming of pulsed X-ray and proton radiography allowed the direct observation of dead zones [4-6].

Previously, we used pulsed X-rays to observe the dead zones in ambient detonating LX-17 with the breakout on the edges measured by streak camera [6]. The “hockey puck” geometry is shown at the right in Figure 1, and it requires the detonation to turn a right angle around an air well. The failure of the detonation occurred at the sharp corner. These results we modeled by adding a “detonation velocity” variable, k , made up of the particle velocity and sound speed in each cell. When $k > k_0$, the explosive detonated; for $k < k_0$, the rate was set to zero. This approach did create dead zones but did not cause cylindrical rate-sticks to fail

without changing the value of k . A setting that caused failure in a rate-stick was too weak to create a dead zone.

There are two differing approaches to modeling. One is Shock Dynamics, an elegant program burn model, which starts with the shape of the front and works back to mathematically describe the conditions of detonation [7,8]. The other is Reactive Flow, which releases the detonation energy on some time scale [9, 10]. The two approaches are conceptually exclusive with the first appealing to mathematicians and the second to chemists. Because of our backgrounds and because detonation is indeed a chemical reaction, we believe that monitoring the reaction rate, however crude the overall scheme may be, is more physical. For us, then, the question is whether a phenomenon is caused by something in the reaction rate, ie. kinetics, or something entirely different. We also note that eventually, the paths of individual chemical reactions will be determined along with their rates so that this approach appears to represent the probable future.

We have also noted that Manfred Held, using the double cylinder method, found that the dead zone for Comp B was considerably larger than for PBX 9502 (see Figure 11 in ref. [6]) [2]. This seemed important because it suggested that something other than kinetics might be involved in creating dead zones. Solving this mystery seemed to be a key step in making our model.

A single reaction rate is used in Ignition & Growth for the entire reaction zone [9]. Failure in this model can be brought on only by raising the power of the pressure to a high value, which then causes other imbalances. The model presented here is a 4 zone/mm simplification of the 8 zones/mm Piece Wise Linear model [11]. This model is calibrated by obtaining a rate constant for a certain pressure, eg. a 5 mm rate stick shows a peak pressure of 33 GPa while a 20 mm rate stick peaks at 36 GPa. At lower pressures, the rate sticks fail and dead zones form. The summation of many results peaked at different pressures produces a rate constant that varies with pressure in unexpected ways.

2 Experimental

Two geometries were used, and both are shown schematically in Figure 1 with the detonation starting downward and turning up to the right. The left side is the double cylinder with a narrow near-ideal LX-14 booster made of five 6.35 mm-radius by 6.35 mm long pellets running into a large test cylinder of radius 25.4 mm and length 50.8 mm. The booster was ignited with a RP-1 detonator. The ball at the corner turn is not real but indicates where the origin of the coordinate system will be in our figures.

The right-side geometry in Figure 1 is the repeat of the previous barrel with 25.4 mm distance from the air well to the outer edge. An air well is sunk into the 1.90 g/cm³ LX-17 main charge, which is driven by a

19.05 mm-radius, 1.80 g/cm³ ultrafine TATB booster. This in turn is driven by a hemispherical detonator, which is made of two layers. The inner layer is 0.93 g/cm³ PETN with a 3.8 mm radius. The outer layer is 1.63 g/cm³ PBX 9407 with a 6.65 mm outer radius.

To display the data, we shall shift the origin to the ball at the corner turn. The angle Θ will indicate the point on the two edges where breakout is measured. We expect straight-ahead behavior from -45° to 0° , with delays occurring in increasing degree from 0° up to the corner at 30.56° and then left to 90° . Three shots used the Figure 1-geometry with cylindrical symmetry. Two of these were bare but one had a steel liner on the inside (but not the bottom) of the air well. The steel thickness was 3.1 mm and the estimated crack between the steel and the explosive was 0.025 mm. A fourth shot was bare but was machined to be square; otherwise, all dimensions were the same as in Figure 1. The shots were: LX-17 cylindrical bare (a repeat of last year), LX-17 cylindrical with a steel liner, LX-17 bare and square, and PBX 9502 cylindrical bare.

Two changes were made from the previous work. First, we used piezoelectric pins of 1.6 mm diameter all along the edges. We did not use an optical pin at the origin so that measurement at the corner where the turn occurred was not possible, because pins cannot be positioned with sufficient accuracy. Instead, we relied on the signal from the pin straight ahead on the axis from the booster (pin 1). Bahl et. al. measured the outward-moving average detonation velocities in LX-17 spheres and found 7.3 mm/ μ s at 19 mm radius and 7.45 mm at 45-50 mm radii, where the velocities are accurate to ± 0.05 mm/ μ s [12]. In our previous work, we had an optical pin at the corner-turn and a piezoelectric pin straight ahead on the axis [6]. The beam of light on the corner pin insured that the corner position was well defined. The average velocity across 21.40 mm of LX-17 to the straight-ahead pin was then

$$U_s = \frac{21.40}{\Delta t + 2.84} \quad (1)$$

where Δt is the unknown lag difference between the axis and the edge of the booster. This gave 7.43 ± 0.06 mm/ μ s for the average velocity from the booster edge to pin 1 (the previously reported 7.64 mm/ μ s was an error). From all this, we shall take this average velocity here to be 7.45 ± 0.15 mm/ μ s, and this generates an error at ± 0.06 μ s for the breakout time and a lag estimate of 0 to 90 ns. This error in the velocity to the pin is larger than the ± 0.4 mm error in setting the pin positions, which produces an angle error or ± 0.5 - 1.5° . The error in reading the time position of the pulses was about ± 0.05 μ s. Our estimate of the overall error for three bare LX-17 and one steel-confined LX-17 times was ± 0.10 μ s except for ± 0.15 μ s from $\Theta = 15^\circ$ to 35° .

A new X-ray system was constructed, using two of the old 450 keV heads plus two new 1 MeV heads so that four pictures were taken on each shot at about 1.5, 3.0, 3.8 and 7-8 μ s after the corner-turn. The radiation dose has been increased to over 10 grays for two of the x-ray channels, to about 7 grays for the third channel, and to 4 grays for the fourth channel. This is the radiation dose per pulse at 1 m with 0.4 mm full-width-half-maximum spot size. The high dose channels consist of two Super 1 MeV Pulsers while the lower dose channels consist of a Super 450 KeV pulser and a regular 450 KeV pulser. All super pulsers are modified to generate higher flux and hence higher dose. The two 1 MeV channels are at 90 degrees to each other. The 450 keV units are 8 degrees to either side of one of the MeV unit forming a close cluster of images. All units project images which are separated into compound film packs.

3 Results

Three double cylinder shots showed no dead zones at all. These were 1.71 g/cc tritonal, 1.86 g/cc LX-04 and 1.70 g/cc Comp B. The last gave the opposite result of the Held experiment and indicated to us that kinetics is probably still the reason for dead zones.

The long-time results for two densities of LX-17 are shown in Figure 2. The increase in density causes the creation of a larger dead zone probably because there are fewer hot spots. Also, the lower density sample has a dead zone with a turnip shape and the high density like a banana. This effect qualitatively occurred in our model when k was increased.

The edge breakout times from the "hockey puck" geometry are listed in Table 1. They include the streak camera results from 2004 at the same angles. The pin results are plotted in Figure 3. We see that all the LX-17 data, including the shot with the steel liner, fall together. Only two angles have standard deviations of the order of the stated accuracy; the rest have smallest standard deviations. Because of this, a lower and upper boundary of times is listed that may be used for the LX-17. The PBX 9502 has smaller times in the corner-turning region, so it is more ideal than the LX-17.

The X-ray transmission photographs of the barrel shots were read directly and the edges of the dead zones digitized. The summary of the inner and outer limits of the dead zone boundaries are listed with the times since the corner-turn began in Table 2.

4 Modeling the TATB Booster

Shock initiation occurs at low pressure, failure/dead zones at intermediate pressure and detonation at high pressure. The ultimate goal is to find a transparent and unified rate structure that handles all three regions simultaneously. The Ignition & Growth model did initiation and detonation with separate packages

[8]. Tang, Johnson and Forest made a hot-spot model in which all three regions are recognized [13], but the model was complex, and it not clear that each region is described by the same overall structure. Here, we seek to describe the failure and detonation regions, which requires running multiple problems simultaneously with identical settings. The explosive model has the rate structure

$$\begin{aligned} \frac{dF}{dt} &= 0, \quad P < P_o \\ \frac{dF}{dt} &= G_2 \left[(P+Q) - P_i \right]^2 (1-F)^{c_2}, \quad P_o < P < P_2 . \\ \frac{dF}{dt} &= G_3 (1-F)^{c_3}, \quad P > P_2 \end{aligned} \quad (2)$$

Region 0 has no reaction, region 2 is failure and region 3 is detonation. It is possible that a separate region 1 for initiation will eventually be included.

We begin with the booster. It probably would have been better to have fired an ideal booster, because modeling the corner-turning is easier in this case. TATB should also be done with reactive flow and this makes the problem more complex. Reactive flow in the booster produces a detonation front lag in the TATB near the air well. This lag allows the front a head start in turning the corner and speeds up the LX-17 detonation. To simulate this, we ran program burn with a fixed contour at the edge of the booster. There is no effect if the lag is 50 ns over 5 degrees or 150 ns lag over 40 degrees. But, if the lag is 150 ns over 10 degrees, the modeled corner-turn is too fast. The actual lag has never been directly measured using a hemispherical detonator. As mentioned above, our inconclusive pin analysis gave a lag with a range of 0 to 90 ns.

We are modeling with JW++ in a 2-D arbitrary Lagrangian-Eulerian (ALE) code with CALE-like properties [10,14]. Our mesh is rectilinear so that the hemispherical reactive flow TATB is painted over it. The detonator is modeled with the two layers in program burn as described above. The detonator is easily lighted in the center zone because of the rectilinear mesh.

It is well known that ram-pressed ultrafine TATB boosters are not at constant density. A representative X-ray tomograph was normalized to 1.80 g/cm³ overall density, because absolute calibration of small density differences is not yet available. The result is shown in Figure 4, where the regions vary from 1.755 to 1.825 g/cc. Figure 4 is arranged in the same geometry as the other figures, so that the top is the open edge for either the corner-turn or the slapper experiment used for our TATB calibration [15]. The detonator is at the upper left. The coordinates of the boundaries were digitized and the common points were made the same between the regions. In the code, the overall booster was created at 1.755 g/cm³ and the other regions were painted on top of that. The necessary coordinates are listed in Table 3. Each region

then needed its own equation of state. The unreacted equation-of-state was determined using the empirical equation in mm/ μ s

$$U_s = C_o + S_I u_p \approx 0.44 \rho_o^3 + 2u_p \quad (3)$$

which is then transformed into the Murnahan form for the model [10].

Each density region has its own JWLS, which are modified using our rules-of-thumb for density changes:

$$\begin{aligned} U_s &\approx \rho_o^{2/3} \\ E_o &\approx \rho_o^{4/3} \\ E_d(2) &\approx \rho_o^{1.80} \\ E_d(4) &\approx \rho_o^{1.70} \\ E_d(7) &\approx \rho_o^{1.65} \end{aligned} \quad (4)$$

where U_s is the detonation velocity, E_o the total detonation energy, $E_d(v)$ the detonation energy at a given relative volume, v , and ρ_o is the initial density.

The size (diameter) effect of 50 μ m TATB was measured at 1.85, 1.80 and 1.70 g/cm³ [16]. We use the observation that the detonation rate is inversely proportional to the inverse of the slope of the inverse radius plot [10]. If we do this, it seems that the rates are about the same at these three densities, and we can use a single rate constant at all our densities.

There is not much data on ultrafine TATB. We have a 1.808 g/cm³, 12.7 mm-radius copper cylinder shot with a detonation velocity of 7.50 mm/ μ s [17]. We also have some 12.7 mm-radius by 20 mm-long cylinders at 1.808 g/cm³ driving 0.54 mm thick copper plates [17], which is probably too small a geometry to get a definitive result. The best test is the hemisphere/booster geometry previously described [15]. Our best overall TATB setting in this model was

$$\begin{aligned} \frac{dF}{dt} &= 0, \quad P < 0.2 \\ \frac{dF}{dt} &= 0.06 \left[(P + Q) - 0.2 \right]^2 (1 - F), \quad 0.2 < P < 30. \\ \frac{dF}{dt} &= 24(1 - F)^{1.5}, \quad P > 30 \end{aligned} \quad (5)$$

The most glaring problem above is the pressure cutoff, which is known to be about 3 GPa from threshold measurements [18,19]. If this value is used, the hemisphere fails. The high-pressure rate of $24 \mu\text{s}^{-1}$ comes directly from the size effect data.

The results of the code runs on the slapper/hemisphere calibration problem are shown in Figure 5. The triangles' size roughly corresponds to the uncertainty of the data. If b_2 is the power of the pressure and G_2 the rate constant in $(\mu\text{s GPa}^{b_2})^{-1}$ in the intermediate pressure range in Eq. (2), then the $b_2, G_2 = 2, 0.06$ curve with the five-density model fits best. The $2, 0.06$ curve with one density fits poorly on the axis. With the five densities, $1, 1.5$ fits very poorly and $2, 0.05$ is too weak, even though it works for the cylinder and the plates. The results of the TATB booster running at $2, 0.06$ are the same in the corner-turning barrel geometry for the five-density model or one density at 1.80 g/cm^3 . Both reach the corner turn at about $1.95 \mu\text{s}$ of code time.

5 Validating the Overall Model

In this paper, we require the following LX-17 matches, all at 4 zones/mm, which is the minimum for this explosive.

- 1) The Cylinder test for LX-17 must agree, but this is easily built into the JWL by setting the proper adiabat energies [20].
- 2) We must generate both the confined and unconfined LX-17 size (diameter) effect curves. The best way is to get detonation velocity agreement of $7.34 \text{ mm}/\mu\text{s}$ for the 4 mm-radius copper cylinder [17], because this fixes the confined line. The unconfined data is sparse at this time and no definite point can be selected, but the curve should lie below the confined line.
- 3) The unconfined barrel corner-turn breakout times must be in fairly good agreement and a dead zone must form. The dead zone should still be present $7 \mu\text{s}$ after the corner turn. A difficult requirement is that the steel-jacketed breakout be essentially similar to the unconfined one, as a result of our single measurement of this type.
- 4) The unconfined cylinder (rate-stick) should detonate at 5 mm radius but fail at 3.75 mm. The rate-stick length is ten times the radius. The confined cylinder (full-wall with wall thickness about $1/5^{\text{th}}$ the explosive radius) should detonate at 4 mm. It should also fail at 3 mm radius, but this requirement is probably too difficult to meet.

The best LX-17 settings we found were

$$\begin{aligned}\frac{dF}{dt} &= 0, \quad P < 10 \\ \frac{dF}{dt} &= 0.011[(P+Q)-10]^{2.7}(1-F), \quad 10 < P < 32. \\ \frac{dF}{dt} &= 40(1-F)^{1.5}, \quad P > 32\end{aligned}\tag{6}$$

We find here that the major knob is the intermediate power of the pressure, b_2 , with the pressure cutoff, P_0 , having a minor effect. The other parameters cause even smaller changes. Various break-out time fits are shown in Figure 6. The value of b_2 began at 2.0 and was raised to 2.7 for the major adjustment. We first set P_0 at 8 GPa because this was the value that came from threshold experiments [18], but this was raised to 10 GPa in the model as the fine adjustment. The $(1 - F)^{1.5}$ term was used to obtain the straight size effect line.

The best curve in Figure 6 is still not right because we needed to turn on the dead-zone parameter a little too much to offset the lag in the booster. The result is that the dead zone has a banana shape, and we want a turnip shape. However, the unconfined dead zone is still there as long as 7 μ s after the corner turn. Figure 6 also shows the model's greatest failure at this time: the steel-confined times are always faster.

The size effect curve is shown in Figure 7. The copper-confined line is excellent but continues to detonate even at the failure point of 3 mm radius. The unconfined curve lies below the confined curve, but there is not presently enough data to be more precise. The unconfined curve runs at 5 mm and fails at 3.75 mm radius.

The model easily works for PBX 9502, which has a JWL with 2% more energy and a 0.5% higher detonation velocity than LX-17. This extra energy causes the front to move more quickly around the dead zone region.

Finally, the model was not designed for shock initiation, but we may test for this anyway. The 50% detonation probability threshold has been measured for 12.7 mm-radius LX-17 from 15 GPa up [18, 21]. We ran from 12.5 GPa, (with extrapolated estimates) through 19 GPa with mylar flyer settings just above threshold. For higher pressures, the delays-to-detonation are too short. The mylar flyer thicknesses and velocities, along with the calculated and measured times to detonation [22-23] are listed in Table 4.

6 Summary

LX-17 and PBX 9502 dead zone data have been extended. The absence of a dead zone in Comp B suggests that kinetics is the cause. We have suggested a single rate format that varies with pressure to describe with some success initiation, failure with dead zone formation and detonation at 4 zones/mm. Further calibration of this model will continue.

7 References

- [1] M. Cox and A. W. Campbell, Corner-Turning in TATB, *Proceedings Seventh Symposium (International) on Detonation*, Annapolis, MD, June 16-19, **1981**, pp. 624-633.
- [2] M. Held, Corner-Turning Distance and Retonation Radius, *Propellants, Explosives, Pyrotechnics* **1989**, *14*, 153-161.
- [3] M. Held, Corner Turning Research Test, *Propellants, Explosives, Pyrotechnics*, **1996**, *21*, 177-180.
- [4] V. A. Komrachov, A. D. Kovtun and Yu. M. Makarov, Use of Pulsed Radiography in Studies of Shock Wave Initiation of TATB, *Combustion, Explosion and Shock Waves*, **1999**, *35* 198-202.
- [5] E. N. Ferm, C. L. Morris, J. P. Quintana, P. Pazuchanic, H. Stacy, J. D. Zumbro, G. Hogan and N. King, Proton Radiography Examination of Unburned Regions in PBX 9502 Corner Turning Experiments, *12th American Physical Society Topical Conference on Shock Compression in Condensed Matter*, Atlanta, GA, June 24-29, 2001, pp. 966-969, **2001**.
- [6] P. Clark Souers, Henry G. Andreski, Charles F. Cook III, Raul Garza, Ron Pastrone, Dan Phillips, Frank Roeske, Peter Vitello and John D. Molitoris, LX-17 Corner Turning, *Propellants, Explosives, Pyrotechnics* **2004**, *29*, 359.
- [7] D. Scott Stewart, Examples of Detonation Shock Dynamics for Detonation Wave Spread Applications, *Proceedings Ninth Symposium (International) on Detonation*, Portland, OR, August 28- September 1, 1989, Naval Surface Weapons Center, Silver Spring, MD, pp. 773-783, **1989**.
- [8] D. C. Swift and S. J. White, Links between Detonation Wave Propagation and Reactive Flow Models, *12th International Detonation Symposium*, San Diego, CA, August 11-16, 2002, pp. 917-926, **2002**.
- [9] E. L. Lee and C. M. Tarver, Phenomenological Model of Shock Initiation in Heterogeneous Explosives, *Phys. Fluid*, **1980**, *23*, 2362-2372.
- [10] P. Clark Souers, Steve Anderson, Estella McGuire and Peter Vitello, JWL++: A Simple Reactive Flow Code Package for Detonation, *Propellants, Explosives, Pyrotechnics*, **2000**, *25*, 54-58.
- [11] Peter Vitello and P. Clark Souers, The Piece Wise Linear Reactive Flow Rate Model, *14th American Physical Society Conference on Shock Compression of Condensed Material*, Baltimore, MD, July 31-August 5, 2005, to be published.
- [12] K. L. Bahl, R. S. Lee and R. C. Weingart, Velocity of Spherically-Diverging Detonation Waves in RX-26-AF, LX-17 and LX-10, *Shock Waves in Condensed Matter-1983*, Elsevier Science Pub., **1984**, pp. 559-562.
- [13] P. K. Tang, J. N. Johnson and C. A. Forest, "Modeling Heterogeneous High Explosive Burn with an Explicit Hot-Spot Process," *Proceedings Eighth Symposium (International) on Detonation*,

Albuquerque, NM, July 15-19, 1985, Naval Surface Weapons Center, Silver Spring, MD, pp. 52-61, **1985**.

- [14] P. Clark Souers, Steve Anderson, Estella McGuire, Michael J. Murphy, and Peter Vitello, Reactive Flow and the Size Effect, *Propellants, Explosives, Pyrotechnics*, **2001**, 26, 26-32.
- [15] Robert L. Druce, P. Clark Souers, Charles Chow, Franklin Roeske, Jr., Peter Vitello and Constantine Hrousis, Detonation in TATB Hemispheres, P. Clark Souers, Henry G. Andreski, Charles F. Cook III, Raul Garza, Ron Pastrone, Dan Phillips, Frank Roeske, Peter Vitello and John D. Molitoris, Detonation in TATB Hemispheres, *Propellants, Explosives, Pyrotechnics*, **2005**, 30, 95-100.
- [16] P. Deneuille, C. Gaudin, Y. de Longueville and J. Mala, Comparison of TATB and DINGU Explosive Properties, *Proceedings Seventh Symposium (International) on Detonation*, Annapolis, MD, June 16-19, 1981, pp. 540-546, **1981**.
- [17] P. Clark Souers, LLNL, unpublished data.
- [18] C. A. Honodel, J. R. Humphrey, R. C. Weingart, R. S. Lee and P. Kramer, Shock Initiation of TATB Formulations, *Proceedings Seventh Symposium (International) on Detonation*, Annapolis, MD, June 16-19, 1981, pp. 425-434, **1981**.
- [19] R. K. Jackson, L. G. Green, R. H. Barlett, W. W. Hofer, P. E. Kramer, R. S. Lee, E. J. Nidick, Jr., L. L. Shaw and R. C. Weingart, Initiation and Detonation Characteristics of TATB, *Proceedings Sixth Symposium (International) on Detonation*, Coronado, CA, August 24-27, 1976, pp. 755-765, **1976**.
- [20] John E. Reaugh and P. Clark Souers, A Constant-Density Gurney Approach to the Cylinder Test, *Propellants, Explosives, Pyrotechnics*, **2004**, 29, 124-128.
- [21] P. Clark Souers, Stan Ault, Rex Avara, Kerry L. Bahl, Ron Boat, Doug Gidding, LeRoy Green, Jim Janzen, Ron Lee, W. C. Weingart, Ben Wu and Kris Winer, Transverse Air Gap Effects in LX-17, submitted *Propellants, Explosives, Pyrotechnics*, **2005**.
- [22] D. C. Dallman and Jerry Wackerle, Temperature-Dependent Shock Initiation of TATB-Based Explosives, *Proceedings Tenth Symposium (International) on Detonation*, Boston, MA, July 12-16, 1993, pp. 130-138, **1993**.
- [23] R. L. Gustavsen, S. A. Sheffield, R. R. Alcon, J. W. Forbes, C. M. Tarver and F. Garcia, Embedded Electromagnetic Gauge Measurements and Modeling of Shock Initiation in the TATB Based Explosives LX-17 and PBX 9502, *Shock Compression of Condensed Matter- 2001*, M. D. Furnish, N. N. Thadhani and Y. Horie, American Institute of Physics, **2002**, pp. 1019-1022.

Acknowledgement

This work was performed under the auspices of the U.S. Department of Energy by the University of California, Lawrence Livermore National Laboratory under Contract No. W-7405-Eng-48.

Table 1. Measured edge breakout times for the “hockey-puck” geometry. The 2004 column is the streak camera data from the first paper; all the rest is this paper’s pin data. The LX-17-all columns create an upper and lower band that summarizes all four LX-17 shots including the steel-confined. Only the PBX 9502 differs. Columns 1 and 2 go together; column 3 refers to all succeeding columns. The summary numbers are the lower and upper bounds of LX-17 times.

Time (μ s)	Breakout Time (μ s)							
	LX-17		2004	LX-17	LX-17	LX-17 summary		PBX 9502
	Angle (deg)	cylinder bare	Angle (deg)	LX-17 bare	cylinder steel	LX-17 square bare	Lower	Upper
79.4	3.77	79.6	3.99	3.98	4.03	3.84	4.04	3.52
67.0	3.79	67.2	3.72	3.75	3.73	3.65	3.85	3.34
48.1	3.65	56.7	3.59	3.66	3.62	3.53	3.73	3.32
41.4	3.75	48.2	3.61	3.68	3.62	3.56	3.76	3.41
36.1	3.99	41.4	3.75	3.74	3.74	3.66	3.96	3.59
31.9	4.23	36.2	3.99	4.07	4.00	3.92	4.22	3.89
26.1	4.30	31.9	4.29	4.35	4.27	4.15	4.45	4.20
13.4	3.81	14.5	3.74	3.85	3.75	3.64	3.94	3.74
-0.8	3.56	0.4	3.50	3.59	3.50	3.44	3.64	3.52
-14.9	3.53	-13.8	3.46	3.56	3.48	3.41	3.61	3.50
-27.4	3.67	-26.5	3.60		3.63	3.53	3.73	3.64
-37.6	3.92	-36.9	3.87	3.94	3.91	3.81	4.01	3.90
-45.6	4.29	-45.1	4.26	4.32	4.28	4.18	4.38	4.23

Table 2. Inner and outer boundaries from X-ray transmission of the dead zones for four samples. The times are since the turn began at the edge of the TATB booster.

Time (μ s)	Distance (mm)										
	Radial	Axial									
LX-17 Cyl. Bare			3.11	0.0	0.9	2.91	0.0	2.2	1.53	0.0	0.2
3.78 μ s	0.0	3.0	outer	5.4	2.3	inner	3.8	2.5	outer	3.5	0.4
inner	3.5	3.0		7.6	3.4		7.7	4.8		6.9	1.9
	6.9	4.2		12.3	9.0		9.3	6.7		7.2	2.9
	8.1	7.4		10.4	10.4		9.1	7.8		6.6	3.6
	6.4	10.1		0.0	10.4		8.1	8.4		4.6	3.7
	2.5	11.2	3.99	0.0	3.1		5.5	8.4		3.2	4.3
	0.0	10.5	inner	5.2	4.5		0.0	8.8		0.0	4.3
3.78	0.0	2.3		6.9	5.9	2.91	0.0	1.8	2.98	0.0	3.7
outer	5.8	3.0		7.4	7.1	outer	5.7	2.3	inner	3.6	3.5
	9.1	4.9		6.4	9.3		10.0	5.6		5.5	5.0
	9.9	7.1		3.5	12.1		11.8	8.6		6.0	7.6
	7.7	9.7		0.0	13.5		6.1	9.1		4.3	8.8
	4.8	11.5	3.99	0.0	2.0		1.8	9.7		0.0	7.7
	0.0	11.7	outer	3.2	2.2		0.0	9.0	2.98	0.0	1.5
7.22	0.0	3.8		8.1	5.4	3.77	0.0	3.3	outer	3.0	1.8
inner	3.5	4.1		7.1	12.4	inner	4.3	3.5		6.2	3.6
	5.8	5.9		3.7	13.8		6.9	5.7		6.8	5.1
	6.0	7.8		0.0	14.0		7.7	7.8		6.8	10.7
	5.6	10.1	7.79	0.0	3.4		6.2	10.7		3.3	12.7
	2.6	11.7	inner	4.6	4.9		0.0	11.4		0.0	11.9
	0.0	12.1		5.8	8.4	3.77	0.0	2.4	3.84	0.0	3.7
7.22	0.0	2.2		5.5	10.1	outer	4.0	2.4	inner	3.9	4.3
outer	6.7	5.0		3.0	12.4		7.3	3.8		5.5	5.9
	7.3	8.7		0.0	13.7		8.2	7.4		4.2	9.0
	5.9	11.0	7.79	0.0	2.4		8.3	11.1		3.2	9.6
	0.0	13.0	outer	4.6	4.2		6.8	12.7		1.5	9.4
LX-17 Cyl. Steel				6.7	5.4		0.0	12.7		0.0	8.0
1.56	0.0	0.9		7.0	9.2	7.88	0.0	2.9	3.84	0.0	2.5
inner	4.8	0.9		3.8	13.1	inner	1.1	3.4	outer	3.7	2.7
	6.6	1.5		0.0	14.8		2.8	6.3		6.7	4.5
	4.3	3.1	LX-17 Square Bare				2.5	8.5		7.2	6.5
	2.2	3.6	1.54	0.0	0.8		1.7	10.5		6.6	8.9
	0.0	3.3	inner	2.9	0.9		0.0	11.3		3.1	10.6
1.56	0.0	0.3		2.7	2.5	7.88	0.0	2.7		0.0	10.6
outer	9.3	0.3		1.8	3.3	outer	1.5	3.2	7.69	0.0	3.4
	6.7	2.8		0.0	3.9		2.7	5.3	inner	2.5	4.3
	3.1	4.8	1.54	0.0	0.4		3.5	8.0		3.5	5.5
	0.0	5.4	outer	1.9	0.4		2.9	10.3		2.2	7.8
3.11	0.0	2.4		3.7	0.0		1.5	11.6		0.0	8.3
inner	4.7	4.1		4.9	0.6		0.0	12.1	7.69	0.0	2.1

7.7	4.8	4.2	2.3	PBX 9502 Cyl. Bare			outer	3.6	3.4
7.9	8.9	1.9	3.8	1.53	0.0	1.2		4.2	4.7
6.1	8.9	0.0	3.9	inner	4.8	1.7		3.9	7.1
0.0	10.0				4.6	2.8		1.5	8.8
					2.1	2.7		0.0	8.9
					0.0	2.2			

Table 3. Boundaries of four density areas inside the 19.05 mm-radius TATB hemisphere. These are superimposed on the 1.755 g/cm³ background.

1.835 g/cm ³		1.780 g/cm ³	
Edge	Axis	Edge	Axis
3.3	-3.5	0.0	-1.6
5.2	-5.4	0.0	-7.2
11.2	-8.3	5.4	-7.2
14.9	-5.0	3.3	-3.5
15.7	-1.6	5.2	-1.3
14.7	-0.8	8.8	-0.8
8.8	-0.8	5.0	-0.7
5.2	-1.3	0.0	-1.6
3.3	-3.5		
1.805 g/cm ³		1.765 g/cm ³	
Edge	Axis	Edge	Axis
3.3	-3.5	0.0	-7.2
5.4	-7.2	0.0	-12.2
7.8	-8.4	8.0	-15.0
9.0	-10.3	12.3	-12.8
11.6	-10.3	15.4	-9.0
15.1	-7.7	17.1	-5.4
17.8	-1.6	17.8	-1.6
14.9	-0.8	15.1	-7.7
15.7	-1.6	11.6	-10.3
15.0	-5.0	9.0	-10.3
11.2	-8.3	7.8	-8.4
5.2	-5.4	5.4	-7.2
3.3	-3.5	0.0	-7.2

Table 4. Run-to-detonation times in LX-17 at threshold conditions

Measured		Model		
Impact Pressure (GPa)	Run-to-Det Time (μs)	Run-to-Det Time (μs)	Flyer Thickness (mm)	Flyer Velocity (mm/ μs)
19.0	0.39	0.1-0.2	0.5	4.1
15.5	0.91	0.5-0.7	1.25	3.6
12.5	2.2	1.4-1.7	7	3.2

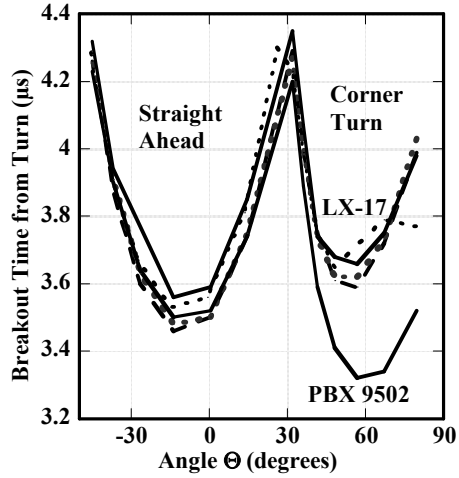


Figure 3. Pin break-out times for LX-17 and PBX 9502 “hockey pucks”. The PBX 9502 is more ideal than the LX-17. The LX-17 lines are: three bare cylinders and square (dotted) and steel-confined (solid line). One bare point at 79° is out of place. Surprisingly, the steel has no effect. The PBX 9502 bare curve is the lowest solid line.

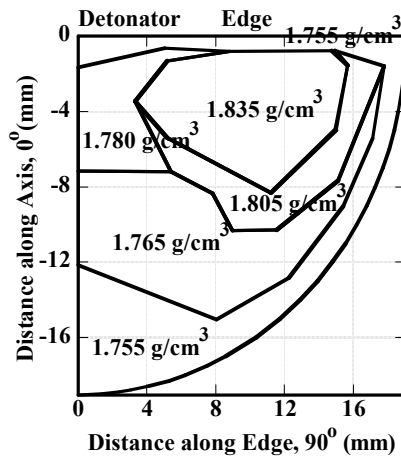


Figure 4. Five-density plot of the TATB booster normalized to an overall density of 1.80 g/cc. The alignment is the same as in the other figures with the open edge at the top. The detonator is at the top left.

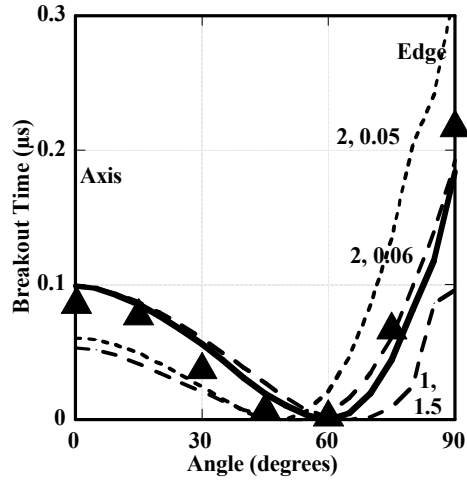


Figure 5. Calculated TATB breakout times for the hemispherical booster with slapper detonator. The average measured data is shown by the triangles. The good fits with b_2 , G_2 values in $(\mu s \cdot GPa^{b_2})^{-1}$ of 2, 0.06 are the single density (dashed) and the five-density (solid). The 2, 0.05 (dashed) and 1, 1.5 (dotted) lines fall outside the data. The five-density curve is the best.

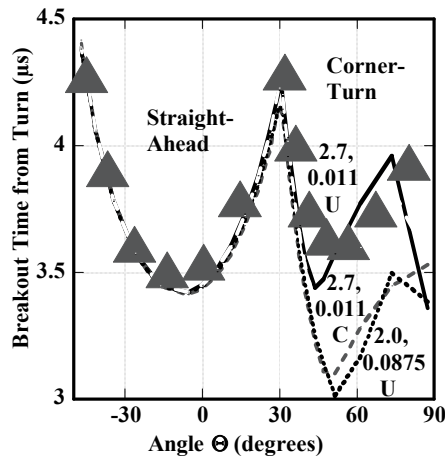


Figure 6. Corner-turning LX-17 breakout times for various code combinations. All of the measured data is averaged by the triangles. The numbers are b_2 , G_2 in $(\mu s \cdot GPa^{b_2})^{-1}$, and P_0 (in GPa). The low dotted line is unconfined 2.0, 0.0875, 8. This is raised to the right place with unconfined 2.7, 0.011, 10. But, including steel drops the curve again with the dashed confined 2.7, 0.011, 10.

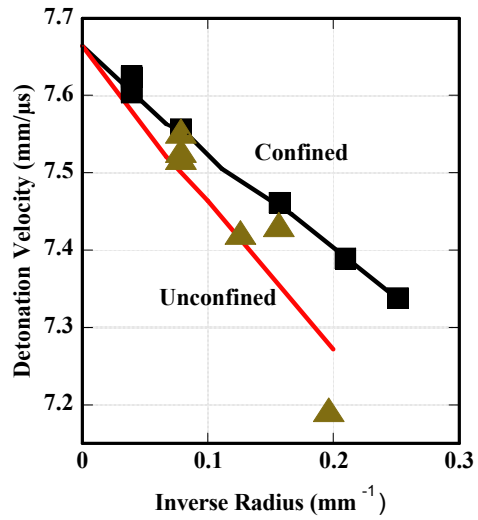


Figure 7. Size effect for LX-17. The measured data is confined (squares) and unconfined (triangles). The lines are the model runs, which are extrapolated to the infinite-radius detonation velocity. More unconfined data is needed.